Inorganic Chemistry

Article

pubs.acs.org/IC

Manganese as a Substitute for Rhenium in CO_2 Reduction Catalysts: The Importance of Acids

Jonathan M. Smieja, Matthew D. Sampson, Kyle A. Grice, Eric E. Benson, Jesse D. Froehlich, and Clifford P. Kubiak*

Department of Chemistry and Biochemistry, University of California, San Diego, 9500 Gilman Drive, Mail Code 0358, La Jolla, California 92093-0358, United States

Supporting Information

ABSTRACT: Electrocatalytic properties, X-ray crystallographic studies, and infrared spectroelectrochemistry (IR-SEC) of Mn(bpy-*t*Bu)$(CO)_3$Br and [Mn(bpy-*t*Bu)$(CO)_3$(MeCN)](OTf) are reported. Addition of Brönsted acids to CO_2-saturated solutions of these Mn complexes and subsequent reduction of the complexes lead to the stable and efficient production of CO from CO_2. Unlike the analogous Re catalysts, these Mn catalysts require the addition of Brönsted acids for catalytic turnover. Current densities up to 30 mA/cm^2 were observed during bulk electrolysis using 5 mM Mn(bpy-*t*Bu)$(CO)_3$Br, 1 M 2,2,2-trifluoroethanol, and a glassy carbon working electrode. During bulk electrolysis at −2.2 V vs SCE, a TOF of 340 s^{-1} was calculated for Mn(bpy-*t*Bu)$(CO)_3$Br with 1.4 M trifluoroethanol, corresponding to a Faradaic efficiency of 100 ± 15% for the formation of CO from CO_2, with no observable production of H_2. When compared to the analogous Re catalysts, the Mn catalysts operate at a lower overpotential and exhibit similar catalytic activities. X-ray crystallography of the reduced species, [Mn(bpy-*t*Bu)$(CO)_3$]$^-$, shows a five-coordinate Mn center, similar to its rhenium analogue. Three distinct species were observed in the IR-SEC of Mn(bpy-*t*Bu)$(CO)_3$Br. These were of the parent Mn(bpy-*t*Bu)$(CO)_3$Br complex, the dimer [Mn(bpy-*t*Bu)$(CO)_3$]$_2$, and the [Mn(bpy-*t*Bu)$(CO)_3$]$^-$ anion.

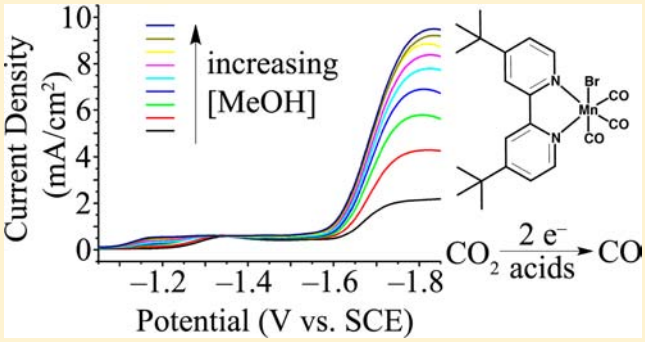

INTRODUCTION

One of the most challenging goals for current and future generations of chemists and engineers is the development of new technologies for the storage of energy. A variety of different technologies including batteries, hydroelectric, thermal, compressed air, and hydrogen production are all frequently discussed as viable options for future energy storage.[1] Another option is the production of liquid fuels from carbon dioxide (CO_2) and water (H_2O). The production of energy-dense fuels could provide a route to nearly carbon neutral energy that would not only fit into existing infrastructure but would enable storage and transport. Achieving this goal will require significant technological advances in carbon dioxide capture (concentration) and catalysis (activation). Many groups are currently working on the issue of carbon dioxide capture from the atmosphere, and advances in that field can be found in several reviews and government reports.[2−7]

Second and third row transition metals have long been the benchmarks for proton or CO_2 reduction catalysts. Transition metals like platinum, palladium, rhodium, and iridium are, in many cases, far superior to their first row counterparts. This trend holds true for synthetic CO_2 reduction catalysts. Many first row transition metal complexes have been reported as catalysts for CO_2 reduction, including metal phthalocyanines (M = Ni, Co, Mn, Cu, Fe), metalloporphyrins (M = Fe, Co, Ni), metal polypyridines (M = Cr, Fe, Co, Ni), and metal cyclams (M = Ni, Co);[8−14] however, the best reported CO_2 electrocatalysts to date are based on Pd,[15−19] Ru,[20] Rh,[21] and Re.[22−25]

Recently, our group has studied catalysts based on the Re(bpy-R)$(CO)_3$X scaffold, where bpy-R is a 4,4′-disubstituted-2,2′-bipyridine and X is either a halide (Cl^- or Br^-) or a solvent molecule accompanied by trfluoromethanesulfonate (triflate, OTf) as a noncoordinating counterion.[23,24,26,27] On the basis of our understanding of the mechanism of the Re catalysts,[27] we were interested in extending our studies to complexes based on the first row counterpart, manganese. Manganese is 1.3 million times more abundant in the Earth's crust than rhenium, at 950 mg Mn/kg crust versus only 7 × 10^{-4} mg Re/kg crust.[28] This fact becomes important when considering not only the cost of scale up but also the environmental ramifications of mining large quantities of raw material.

Received: November 1, 2012
Published: February 18, 2013

   dx.doi.org/10.1021/ic302391u | *Inorg. Chem.* 2013, 52, 2484−2491

In 2011, Deronzier and co-workers reported that Mn(bpy)-$(CO)_3Br$ and Mn(dmbpy)$(CO)_3Br$ (where bpy = 2,2′-bipyridine and dmbpy = 4,4′-dimethyl-2,2′-bipyridine) were electrocatalysts for the reduction of CO_2 to CO with reasonable efficiencies, selectivities, and stabilities when H_2O was present in the electrochemical cell.[29] The Mn complexes show no activity toward CO_2 reduction without the addition of an external proton source. Compared to their Re counterparts,[22] the Mn catalysts also showed lower current densities and lower stabilities, as observed during bulk electrolysis.

Herein we describe the synthesis, electrochemistry, infrared spectroelectrochemistry, and X-ray crystallography of modified manganese catalysts. Mn(bpy-*t*Bu)$(CO)_3Br$ and [Mn(bpy-*t*Bu)$(CO)_3$(MeCN)](OTf) (where bpy-*t*Bu = 4,4′-di-*tert*-butyl-2,2′-bipyridine) were fully characterized and showed high selectivity, efficiency, and stability for the reduction of CO_2 to CO in the presence of H_2O, methanol (MeOH), and 2,2,2-trifluoroethanol (TFE). Notably, these complexes have similar catalytic activity and reduce CO_2 at less overpotential (a gain of 300 mV) when compared to their rhenium counterparts. This work confirms and improves upon Deronzier's work on Mn(bpy)$(CO)_3Br$ and Mn(dmbpy)$(CO)_3Br$.

RESULTS AND DISCUSSION

Synthesis and Characterization. Synthesis of Mn(bpy-*t*Bu)$(CO)_3Br$ (**1**) was performed analogously to a previously reported procedure.[30] The product was characterized by ^1H NMR, FTIR, elemental analysis, and X-ray crystallography. [Mn(bpy-*t*Bu)$(CO)_3$][K(18-crown-6)] (**2**) was prepared by the reduction of **1** in tetrahydrofuran (THF) by KC_8 (2.1 equiv) in the presence of 18-crown-6 (2.5 equiv). The product was characterized by ^1H NMR, FTIR, and X-ray crystallography (see Experimental Section). [Mn(bpy-*t*Bu)$(CO)_3$(MeCN)]-(OTf) (**3**) was prepared by reacting **1** with silver trifluoromethansulfonate (AgOTf) and characterized by ^1H NMR, FTIR, and elemental analysis.

X-ray Crystallographic Studies. Recently, we have had success growing crystals of both the parent and anionic species of Re(bpy-R)$(CO)_3X$ complexes.[27,31] X-ray quality crystals of complex **1** were grown by vapor diffusion of pentane into a tetrahydrofuran (THF) solution of the complex (Figure 1). The crystal structure of the doubly reduced species, [Mn(bpy-*t*Bu)$(CO)_3$][K(18-crown-6)] (**2**), was also obtained (Figure 2). Reduction of **1** by KC_8 (2.1 equiv) in the presence of 18-crown-6 afforded **2**. 18-crown-6 was added to inhibit potassium coordination to the carbonyls of the anionic Mn complex. Crystals of the anion were grown by vapor diffusion of pentane into THF and crystallized in the space group $P2(1)/c$ with two independent molecules in the unit cell. Reduction of the compound results in the loss of the bromide, forming the five-coordinate unsaturated complex. The geometry of one of the anionic molecules in the asymmetric unit cell ($Z' = 2$) is intermediate between square pyramidal and trigonal bipyramidal with a $\tau_5 = 0.53$. On this scale, a perfect square pyramid has a $\tau_5 = 0$ and a perfect trigonal bipyramid has a $\tau_5 = 1$.[32]

The structure of **2** is very similar to the structure of [Re(bpy-*t*Bu)$(CO)_3$][K(18-crown-6)], where the molecule is also five-coordinate and has a $\tau_5 = 0.46$.[27] The X-ray crystal structure of **2** is nearly identical to that of the DFT-calculated structure (see Supporting Information). Of the two molecules in the asymmetric unit cell for **2**, one has a slight disorder in the rotation of the facial carbonyls (Figure S6), suggesting that there may be a shallow barrier for rotation between the square pyramidal and the trigonal bipyramidal forms.

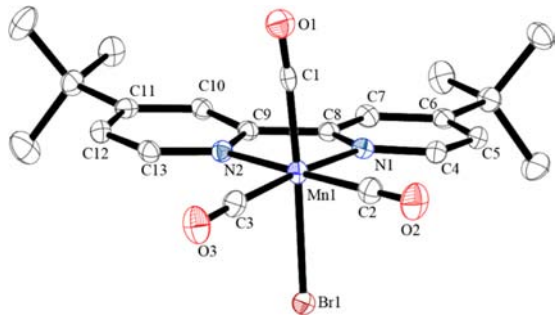

Figure 1. Molecular structure of Mn(bpy-*t*Bu)$(CO)_3Br$ (**1**), with hydrogen atoms omitted for clarity. One of two of the molecules in the asymmetric unit ($Z' = 2$) is shown, with ellipsoids set at the 50% probability level. Relevant distances (Å) and bond angles (°): Mn1−Br1, 2.5101(5); Mn1−N1, 2.045(2); Mn1−N2, 2.040(2); Mn1−C1, 1.848(2); Mn1−C2, 1.812(3); Mn1−C3, 1.806(2); O1−C1, 1.091(3); O2−C2, 1.144(4); O3−C3, 1.141(3); N1−C4, 1.344(3); N1−C8, 1.349(3); N2−C9, 1.357(3); N2−C13, 1.343(3); C4−C5, 1.386(3); C5−C6, 1.397(4); C6−C7, 1.394(4); C7−C8, 1.397(3); C8−C9, 1.480(3); C9−C10, 1.388(4); C10−C11, 1.394(3); C11−C12; 1.395(3); C12−C13, 1.378(4); Br1−Mn1−N1, 87.07(6); Br1−Mn1−N2; 90.06(6); Br1−Mn1−C1, 175.68(8); Br1−Mn1−C2, 88.90(9); Br1−Mn1−C3, 85.66(8); N1−Mn1−N2, 78.42(8); N1−Mn1−C1, 97.24(9); N1−Mn1−C2, 97.0(1); N1−Mn1−C3, 171.4(1); N2−Mn1−C1, 90.54(9); N2−Mn1−C2, 175.4(1); N2−Mn1−C3, 97.0(1); C1−Mn1−C2, 90.8(1); C1−Mn1−C3, 90.0(1); C2−Mn1−C3, 87.4(1).

Comparison of the bpy ligands in the crystal structures of **1** and **2** reveals significant shortening of the inter-ring C−C bond in **2** as compared to **1** (1.412(9) Å and 1.478(8) Å, respectively). This shortened inter-ring C−C bond is consistent with the structure of Hartl's [Mn(bpy)$(CO)_3$][Na(bpy)·Et_2O], with an inter-ring C−C bond of 1.418(3) Å.[33] Bond length alternation in the bpyridine ligand of **2** can also be clearly observed (Figure 2). This bond length alternation is similar to what is seen in the structures of isolated reduced bpys and suggests significant electron density on the bpy ligand.[34] The DFT-calculated highest occupied molecular orbital (HOMO) of **2** was found to be a hybrid involving both the ligand and the metal center, containing substantial bpy π^* character (Figure S7), very similar to the $[Re(bpy\text{-}tBu)(CO)_3]^-$ calculated HOMO.[27]

Electrochemistry. Electrochemical experiments were performed to evaluate the electrocatalytic properties of **1** and **3**. The cyclic voltammetry of **1** in dry acetonitrile under an atmosphere of argon is very similar to the previously reported electrochemistry of Mn(bpy)$(CO)_3Br$ and Mn(dmbpy)-$(CO)_3Br$ and is displayed in Figure 3.[29] The cyclic voltammogram (CV) consists of two irreversible, one-electron reduction waves. The first wave is at −1.39 V vs SCE and the second reduction is at −1.57 V vs SCE. The second reduction leads to the catalytically active $[Mn(bpy\text{-}tBu)(CO)_3]^-$ anion. A large oxidation wave is observed in the CV of this complex at −0.30 V vs SCE. This wave is attributed to the oxidative cleavage of the Mn−Mn dimer formed upon the first reduction of the complex. The electrochemistry of [Mn(bpy-*t*Bu)-$(CO)_3$(MeCN)](OTf) (**3**) is very similar to **1**, with reduction potentials at −1.28 and −1.56 V vs SCE. Complex **3** is freely diffusing in solution according to the Randles−Sevcik equation

dx.doi.org/10.1021/ic302391u | *Inorg. Chem.* 2013, 52, 2484−2491

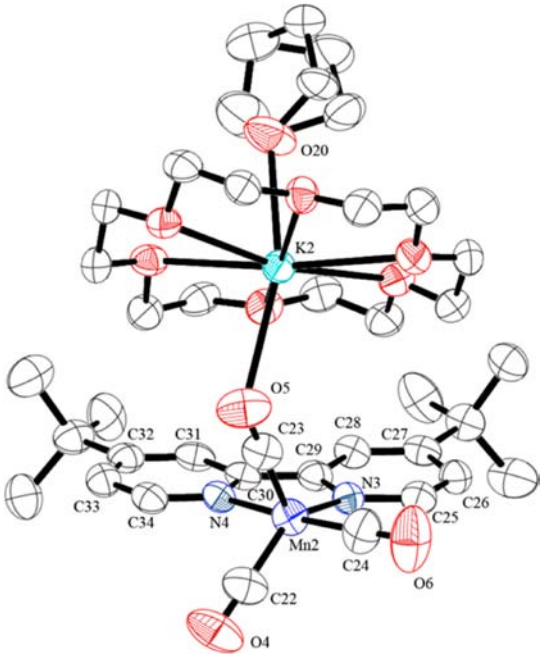

Figure 2. Molecular structure of [Mn(bpy-*t*Bu)(CO)$_3$][K(18-crown-6)(THF)] (**2**), with hydrogen atoms removed for clarity. One of the two molecules in the asymmetric unit (Z' = 2) is shown, with ellipsoids set at the 50% probability level. The other molecule in the asymmetric unit contains positional disorder of the carbonyls around the metal center, with the major occupancy modeled at 69%, and is shown in Figure S6. Relevant distances (Å) and bond angles (°): Mn2−N3, 1.981(5); Mn2−N4, 1.991(5); Mn2−C22, 1.773(9); Mn2−C23, 1.784(8); Mn2−C24, 1.766(9); K2−O5, 2.845(6); K2−O20, 2.709(6); O4−C22, 1.17(1); O5−C23, 1.185(9); O6−C24, 1.19(1); N3−C25, 1.375(9); N3−C29, 1.395(9); N4−C30, 1.386(9); N4−C34, 1.360(9); C25−C26, 1.35(1); C26−C27, 1.44(1); C27−C28, 1.44(1); C28−C29, 1.40(1); C29−C30, 1.41(1); C30−C31, 1.43(1); C31−C32, 1.36(1); C32−C33, 1.43(1); C33−C34, 1.35(1); C22−Mn2−C23, 97.2(4); C22−Mn2−C24, 91.3(4); C23−Mn2−C24, 88.9(4); N3−Mn2−N4, 78.8(2); N3−Mn2−C22, 122.9(3); N3−Mn2−C23, 122.9(3); N3−Mn2−C24, 93.0(3); N4−Mn2−C22, 95.8(3); N4−Mn2−C23, 94.6(3); N4−Mn2−C24, 171.7(3).

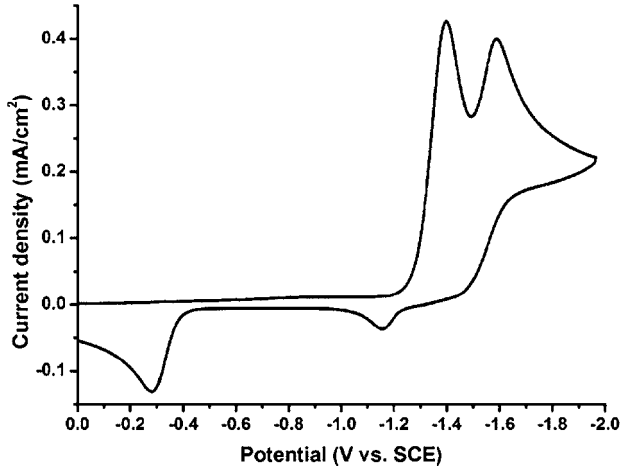

Figure 3. Cyclic voltammogram of 1 mM Mn(bpy-*t*Bu)(CO)$_3$Br (**1**) in MeCN with 0.1 M TBAH as the supporting electrolyte under an atmosphere of argon showing two irreversible one-electron reductions of the complex. Working electrode is a 1 mm diameter glassy carbon, counter electrode is a platinum wire, and pseudoreference is a silver wire with ferrocene added as an internal reference.

(Figure S1).[35] The scan rate dependence of complex **1** is very similar to **3**.

It is useful to compare the electrochemistry of complexes **1** and **3** to that of the closely related Re(bpy-*t*Bu)(CO)$_3$Cl that we have reported previously.[24] The Re complex also exhibits two single electron reductions. The first reduction of the Re complex is reversible when scanning is stopped before reaching the second reduction potential. When scanning through the second reduction potential, this first reduction becomes quasi-reversible. The first reduction of the Mn complexes, however, is irreversible regardless of the switching potential or the scan rate up to 12 V/s, indicating that bromide loss upon first reduction is rapid and irreversible. Another major difference is the large oxidation peak at −0.30 V vs SCE in the Mn complexes that is not present in either Re(bpy-R)(CO)$_3$X complexes or in Re(bpy-*t*Bu)(CO)$_3$(L)(OTf) (where L = MeCN or pyridine). This difference reflects the enhanced tendency of Mn complexes to dimerize upon single electron reduction compared to Re complexes. In addition, the two reductions of the Mn complexes are closer in potential to each other than those of the Re analog. The two reductions of **1** and **3** are separated by only 180−280 mV, while the two reductions of Re(bpy-R)(CO)$_3$X complexes (where R = H, Me, *t*Bu, or OMe and X = Cl$^-$ or Br$^-$) are separated by 300−400 mV, depending on bpy substitution. It is important to note that the 300 mV anodic shift of the second reduction for the Mn complexes compared to the analogous Re complexes represents a significant decrease in overpotential to form the species that is involved in reduction of CO_2 to CO. This shift in potential may also be the reason why added proton sources are required for catalytic turnover to occur, a phenomenon not observed for Re complexes and one that will be discussed further (*vide infra*).

Infrared Spectroelectrochemistry. Infrared spectroelectrochemistry (IR-SEC) of complex **1** under N_2 was performed to gain insight into the precursors of the active catalyst. Three major species were observed in the progression through both reductions of complex **1** and are shown in Figure 4. In its

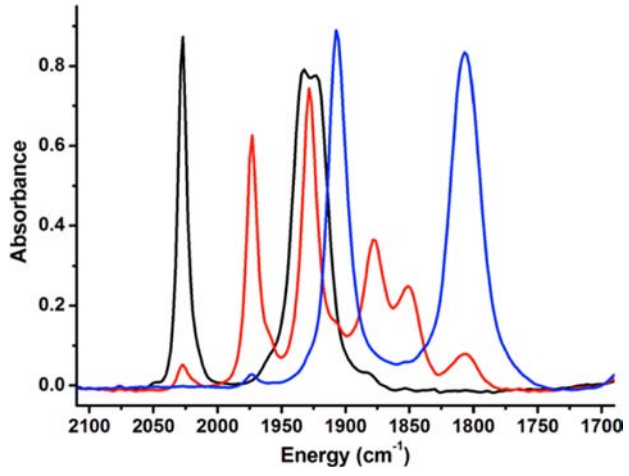

Figure 4. Three species are observed in the IR-SEC of complex **1** in MeCN under an atmosphere of N_2. The rest species (black, **1**) has three characteristic ν(CO) stretches at 2028, 1933, and 1923 cm^{-1}. The singly reduced species (red) forms a dimer rapidly and completely upon reduction and has ν(CO) stretches at 1973, 1928, 1878, and 1850 cm^{-1}. Finally, the doubly reduced species (blue) has only two ν(CO) stretches at 1907 and 1807 cm^{-1}.

dx.doi.org/10.1021/ic302391u | *Inorg. Chem.* 2013, 52, 2484−2491

resting state, complex **1** has three characteristic ν(CO) stretches for facially coordinated tricarbonyl complexes at 2028, 1933, and 1923 cm^{-1}. Upon one-electron reduction of the parent complex, complete formation of the Mn−Mn dimer, $[Mn(bpy\text{-}tBu)(CO)_3]_2$, is observed with no prior intermediates. This implies that loss of bromide, followed by dimerization, occurs rapidly upon reduction. The ν(CO) bands for the dimer species appear at 1973, 1928, 1878, and 1850 cm^{-1}. These ν(CO) bands match well with those previously reported for both $[Mn(bpy)(CO)_3]_2$ and $[Re(bpy)(CO)_3]_2$.[36,37] Upon further reduction, a third species is formed with ν(CO) bands at 1907 and 1807 cm^{-1}. This is indicative of the $[Mn(bpy\text{-}tBu)(CO)_3]^-$ anionic species that acts as the active catalyst for CO_2 reduction. The ν(CO) bands also correlate well with those for the $[Mn(bpy\text{-}tBu)(CO)_3][K(18\text{-crown-}6)]$ species produced by the chemical reduction of **1** using KC_8 (1905 and 1805 cm^{-1}). It is interesting that these ν(CO) stretches are shifted by 40 cm^{-1} lower in energy when compared to the equivalent bands for $[Re(bpy\text{-}tBu)(CO)_3]^-$ reported previously.[24] Bond length alternation in the bpy ring,[37] along with DFT calculations, indicate that significant electron density still resides on the bpy ring for complex **2**, but the very low energy CO stretching frequencies indicate that M−CO back bonding is significantly increased as compared to the analogous Re complex.

Rotating Disk Electrochemistry. Rotating disc electrode (RDE) experiments were carried out on $[Mn(bpy\text{-}tBu)(CO)_3(MeCN)](OTf)$ (**3**) in order to determine the diffusion coefficients of the complex. The data obtained from these experiments display Levich−Koutecky behavior (Figure S2). The Levich−Koutecky equation was used to obtain diffusion coefficients from that data (eq 1).[38]

$$i_L = (0.620)nFAD^{2/3}\omega^{1/2}\upsilon^{-1/6}C \quad (1)$$

In the above equation, i_L is the Levich current from the rotating disc experiment, n is the number of electrons (1 in this case), F is Faraday's constant, A is the electrode area, D is the diffusion coefficient, ω is the rotation rate, υ is the kinematic viscosity of the solution, and C is the concentration of the analyte in solution. These data yielded diffusion coefficients of 1.1×10^{-5} cm^2/s for $[Mn(bpy\text{-}tBu)(CO)_3(MeCN)](OTf)$ and 4.4×10^{-6} cm^2/s for the singly reduced species. The value for the parent species is reasonable when compared to diffusion coefficients for similar complexes in the literature.[24,39] The diffusion coefficient for the singly reduced species, however, indicates that the complex forms a dimer upon single reduction. This result is in agreement with our IR-SEC results, as well as results previously reported by Hartl and co-workers.[40] Rotating disk electrochemistry data for **1** were irreproducible. However, the diffusion coefficients for the electrochemistry of **1** are likely to be very similar to those calculated from the study of **3**.

Electrocatalysis. The electrocatalytic properties of **1** and **3** (1 mM in MeCN) were studied in a custom-made, single-compartment, airtight cell with a glassy carbon working electrode, Pt counter electrode, and a Ag wire pseudoreference electrode separated from the main compartment by a Vycor tip. A 10 min sparge of the acetonitrile solution with "bone dry" carbon dioxide yielded a gas-saturated solution (ca. 0.28 M).[41] The electrochemistry of complexes **1** and **3** did not change significantly under CO_2 in dry acetonitrile. Addition of weak Brönsted acids to **1** (H_2O, MeOH, or TFE), however, resulted in an increase in the current at the second reduction potential, representing catalytic current for the reduction of CO_2 to CO. This increase in current can be seen at approximately −1.57 V vs SCE in Figure 5 (MeOH addition) and in Figures S3 and S4 (addition of H_2O and TFE, respectively). Addition of weak Brönsted acids to **3** resulted in very similar trends.

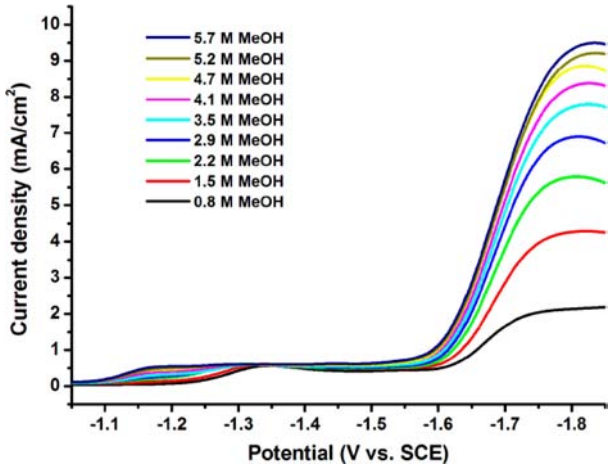

Figure 5. Linear scan voltammograms showing the electrocatalytic reduction of CO_2 to CO by 1 mM $Mn(bpy\text{-}tBu)(CO)_3Br$ (**1**) in acetonitrile with addition of MeOH. The solution is under an atmosphere of, and saturated with (ca. 0.28 M), carbon dioxide. Electrochemical conditions were 0.1 M TBAH as supporting electrolyte, 1 mm diameter glassy carbon working electrode, Pt wire counter electrode, and Ag wire reference electrode separated from the bulk solution by a Vycor tip.

Addition of H_2O to a 1 mM solution of **1** under CO_2 resulted in an increase in catalytic current up to 5.9 mA/cm^2 (i_{cat}/i_p = 12) at 2.7 M H_2O (ca. 5% by volume) before eventually dropping with additional H_2O. The shape of the reduction waves before the catalytic wave changes significantly upon H_2O addition, and changes in the first reduction potential are observed in the presence of MeOH and TFE as well. The shift in the first reduction toward more positive potentials in the presence of weak Brönsted acids can be attributed to the solvolysis of the Mn−Br bond and formation of $Mn(bpy\text{-}tBu)(CO)_3(S)]^+$ species.[29] The fact that Brönsted acids are necessary for catalytic activity suggests that catalysis will not occur unless protonation of a M−CO_2 adduct occurs. In the analogous Re system, the addition of weak Brönsted acids increases catalytic current and stabilizes the Re−CO_2 adduct, likely facilitating the cleavage of one C−O bond leading to CO formation.[42] However, in the Re system, catalysis still occurs in the absence of added Brönsted acids, likely due to scavenging of protons from solvent or electrolyte.

The addition of stronger Brönsted acids leads to higher current densities in the CVs of **1** under CO_2, similar to the trend observed with $Re(bpy\text{-}R)(CO)_3X$ complexes.[27,42] CVs with added MeOH reach 13 mA/cm^2 (i_{cat}/i_p = 26) at 5.8 M MeOH and 1 mM catalyst. CVs with added TFE reach 16 mA/cm^2 (i_{cat}/i_p = 42) at 1.4 M TFE and 1 mM catalyst, and 47 mA/cm^2 at 5 mM catalyst (Figure S5). A summary of i_{cat}/i_p for the addition of all three Brönsted acids is found in Table 1 (i_{cat}/i_p calculated values include a correction for the concentration change of the catalyst). The high current densities in the cyclic voltammograms of **1** under CO_2 with added Brönsted acids rival those of Re complexes at similar conditions.[27]

In order to compare the activities of this Mn system with the previously reported Re catalysts, eq 2, the equation for catalytic

dx.doi.org/10.1021/ic302391u | Inorg. Chem. 2013, 52, 2484−2491

Table 1. Comparison of i_{cat}/i_p Values for 1 mM of Mn(bpy-*t*Bu)(CO)$_3$Br (1) and [Re(bpy-*t*Bu)(CO)$_3$(MeCN)](OTf) in MeCN (Under Identical Conditions That Give Maximum Mn(bpy-*t*Bu)(CO)$_3$Br (1) Activity). Solutions Are Saturated with (ca. 0.25−0.27 M)[a] and under an Atmosphere of CO_2 with Added Brönsted Acids

		Mn(bpy-*t*Bu)(CO)$_3$Br (**1**)		[Re(bpy-*t*Bu)(CO)$_3$(MeCN)](OTf)		
Brönsted acid	[acid][b] (M)	i_{cat}/i_p[c]	TOF (s^{-1})	i_{cat}/i_p[d,e]	TOF (s^{-1})	TOF_{Mn}/TOF_{Re}
H_2O	3.1	25	120	5.4	5.7	21
MeOH	5.8	26	130	22	94	1.4
TFE	1.4	42	340	46	410	0.83

[a] $[CO_2]$ is ca. 0.26 M in 3.1 M H2O, 0.25 M in 5.8 M MeOH and 0.27 M in 1.4 M TFE.[35] [b] [acid] at highest i_{cat}/i_p for Mn(bpy-tBu)(CO)$_3$Br (**1**). [c] i_{cat}/i_p values include a correction for the concentration change of the catalyst. [d] These values are not maximum i_{cat}/i_p values for [Re(bpy-*t*Bu)(CO)$_3$(MeCN)](OTf). [e] Values taken from Wong et al.[42]

current, and eq 3, which describes current response in the absence of catalyst substrate, can both be used to estimate catalytic activity. If eq 3 is divided by eq 2, the resulting equation can be reorganized to solve for turnover frequency (TOF) (eq 4).

$$i_{cat} = n_{cat}FA[C_{cat}](D_c k_{cat}[S]^y)^{1/2} \quad (2)$$

$$i_p = 0.4463\left(\frac{F}{RT}\right)^{1/2} n_p^{3/2} A D_c^{1/2}[C_p]v^{1/2} \quad (3)$$

$$\mathrm{TOF} = k_{cat}[S] = \frac{Fvn_p^3}{RT}\left(\frac{0.4463}{n_{cat}}\right)^2\left(\frac{i_{cat}}{i_p}\right)^2 \quad (4)$$

In these equations, i_{cat} is catalytic current, i_p is peak current in the absence of catalysis, n_{cat} is the number of electrons in the catalytic transformation (2 for the transformation of CO_2 into CO), F is Faraday's constant, R is the universal gas constant, T is temperature in Kelvin, A is the surface area of the electrode, $[C_{cat}]$ is the catalyst concentration under catalytic conditions (at peak i_{cat}/i_p the concentration of the catalyst is less because of the added volume of the protic additive), $[C_p]$ is the catalyst concentration without substrate, D_c is the diffusion constant of the species prior to the catalytically active species, k_{cat} is the rate constant of the catalytic reaction, $[S]$ is the substrate concentrations, y is the order of the substrates in the reactions ($[CO_2]^1[HX]^2$ in this case), and v is scan rate (0.1 V/s). We note the shortcomings of these equations, but we believe the equations are appropriate in this context due to the strong similarities of the Mn and Re systems. These equations assume that the catalytic reaction is under pseudo-first-order conditions, with an excess of substrate compared to the catalysts. In addition, the k_{cat} is specific to the conditions of the system (i.e., k_{cat} at a given concentration of MeOH will not be the same as k_{cat} at the same concentration of H_2O or TFE). Surface area cancels out because the same electrode was used, and in the current treatment D_c cancels out because we are assuming that the diffusion coefficient does not significantly change with the addition of the acid or CO_2.

Using eq 4, we can obtain TOF values of 130 s^{-1} and 340 s^{-1} for catalyst **1** under peak i_{cat}/i_p conditions with 5.8 M MeOH and 1.4 M TFE, respectively. In comparison, using eq 4 and previously reported values reported for CO_2 reduction, we can obtain TOF values of 94 s^{-1} (i_{cat}/i_p = 22) and 410 s^{-1} (i_{cat}/i_p = 46) for [Re(bpy-*t*Bu)(CO)$_3$(MeCN)](OTf) with 5.8 M MeOH and 1.4 M TFE, respectively.[27] This result indicates that the Mn catalyst **1** is slightly more active than [Re(bpy-*t*Bu)(CO)$_3$(MeCN)](OTf) with 5.8 M MeOH (TOF_{Mn}/TOF_{Re} = 1.4) and slightly less active than [Re(bpy-*t*Bu)(CO)$_3$(MeCN)](OTf) with 1.4 M TFE (TOF_{Mn}/TOF_{Re} = 0.83). However, at peak i_{cat}/i_p conditions, the [Re(bpy-*t*Bu)(CO)$_3$(MeCN)](OTf) catalyst reaches a TOF value of 340 s^{-1} (i_{cat}/i_p = 42) and 570 s^{-1} (i_{cat}/i_p = 54) with 9.9 M MeOH and 1.6 M TFE, respectively.[27] At the peak i_{cat}/i_p conditions for both catalysts, Mn catalyst **1** is approximately 2 times less active than [Re(bpy-*t*Bu)(CO)$_3$(MeCN)](OTf) with added MeOH or TFE. A summary of TOF values for Mn catalyst **1** and [Re(bpy-*t*Bu)(CO)$_3$(MeCN)](OTf) at conditions that give peak i_{cat}/i_p conditions for Mn catalyst **1** for the addition of all three Brönsted acids is shown in Table 1. A comparison of TOF values at peak i_{cat}/i_p conditions for both Mn catalyst **1** and [Re(bpy-*t*Bu)(CO)$_3$(MeCN)](OTf) for the addition of all three Brönsted acids is found in Table 2.

Table 2. Comparison of Peak i_{cat}/i_p Values for Both Mn(bpy-*t*Bu)(CO)$_3$Br (1) and [Re(bpy-*t*Bu)(CO)$_3$(MeCN)](OTf) in MeCN (1 mM in Each Catalyst). Solutions Are Saturated with (ca. 0.19−0.28 M)[a] and under an Atmosphere of CO_2 with Added Brönsted Acids

	Mn(bpy-*t*Bu)(CO)$_3$Br (**1**)			[Re(bpy-*t*Bu)(CO)$_3$(MeCN)](OTf)			
Brönsted acid	[acid][b] (M)	i_{cat}/i_p[c]	TOF (s^{-1})	[acid][d] (M)	i_{cat}/i_p[c,e]	TOF (s^{-1})	TOF_{Mn}/TOF_{Re}
none	0.0	1.0	0	0.0	3.3	2.1	
H_2O	3.1	25	120	10	9.0	16	7.5
MeOH	5.8	26	130	9.9	42	340	0.38
TFE	1.4	42	340	1.6	54	570	0.60

[a] $[CO_2]$ is ca. 0.28 M in dry MeCN, 0.19 M in 10 M H2O, 0.22 M in 9.9 M MeOH and 0.27 M in 1.6 M TFE.[35] [b] [Acid] at highest i_{cat}/i_p for Mn(bpy-tBu)(CO)$_3$Br (**1**). [c] i_{cat}/i_p values include a correction for the concentration change of the catalyst. [d] [Acid] at highest i_{cat}/i_p for [Re(bpy-*t*Bu)(CO)$_3$(MeCN)](OTf). [e] Values taken from Wong et al.[42]

Notably, at low MeOH or TFE concentrations, the rhenium catalyst clearly outperforms the Mn catalyst because these acids are necessary for turnover in the Mn case, whereas the rhenium catalyst is active in "dry" acetonitrile.

Unlike with added MeOH or TFE, Mn catalyst **1** clearly outperforms [Re(bpy-*t*Bu)(CO)$_3$(MeCN)](OTf) with added H_2O. A TOF value of 120 s^{-1} was calculated for Mn catalyst **1** under peak i_{cat}/i_p conditions (3.1 M H_2O). Similarly, a TOF value of only 5.7 s^{-1} (i_{cat}/i_p = 5.4) was calculated for [Re(bpy-*t*Bu)(CO)$_3$(MeCN)](OTf) with 3.1 M H_2O (Table 1). Even at peak i_{cat}/i_p conditions, the [Re(bpy-*t*Bu)(CO)$_3$(MeCN)](OTf) catalyst only reaches a TOF value of 16 s^{-1} with H_2O (10 M).[27] At peak i_{cat}/i_p conditions for both catalysts, Mn catalyst **1** is approximately 7.5 times more active than [Re(bpy-*t*Bu)(CO)$_3$(MeCN)](OTf) with added H_2O.

Bulk electrolysis (at −2.2 V vs SCE) monitored by gas chromatography indicates that no hydrogen is formed and a Faradaic efficiency of 100 ± 15% is achieved for the formation of CO from CO_2 at 5 mM catalyst with added TFE (Figure 6). The catalyst was able to sustain current densities as high as 30 mA/cm^2 with added TFE for a period of more than three hours

dx.doi.org/10.1021/ic302391u | Inorg. Chem. 2013, 52, 2484−2491

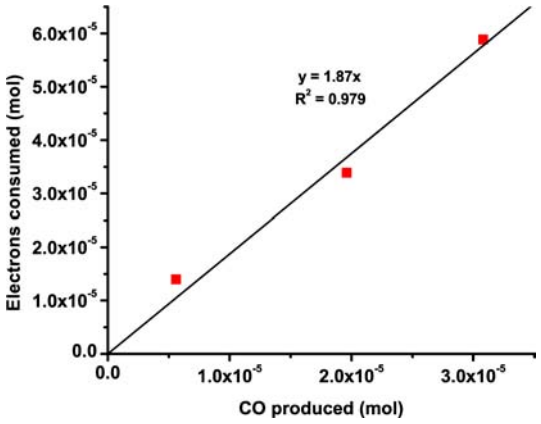

Figure 6. Production of CO from CO_2 by 5 mM Mn(bpy-*t*Bu)$(CO)_3$Br (**1**) during bulk electrolysis at −2.2 V with 0.8 M TFE. The slope of ca. 2 represents a Faradaic efficiency of 100 ± 15%. Bulk electrolysis of this solution showed a 30% current loss over the first 20 min as is usual to reach steady state, but no significant degradation over a period of more than three hours thereafter.

with very little loss of activity (ca. 30% over the first 30 min, followed by stable current).

In order to more accurately compare the activity of the Mn catalyst reported here with other previously reported catalysts, Savéant's method[9,43] for calculating TOF from bulk electrolysis experiments was utilized (see Supporting Information for details). This analysis leads to a calculated TOF of 267 s^{-1} for catalyst **1** in the presence of 1.4 M TFE. The activity for Mn catalyst **1** in the presence of TFE is approximately 300 times more active than Mn(bpy)$(CO)_3$Br in the presence of 5% H_2O (0.89 s^{-1}) and is approximately 7 times less active than Re(bpy)$(CO)_3$Cl in DMF/2 M H_2O (1016 s^{-1}).[9,29] The activity of Mn catalyst **1** is on the same order of magnitude as the activity of Ni(cyclam) in 1:4 H_2O/MeCN (158 s^{-1}) using this analysis.[9,11]

In addition to catalytic activity, Savéant's method for calculating equilibrium overpotential[9] can be applied to the Mn catalyst **1**. Equilibrium overpotential is calculated by taking the difference between the standard potential of the CO_2/CO couple (estimated to be −0.90 V vs SCE) and the operating electrode potential (−1.60 V vs SCE). Here, we calculate an equilibrium overpotential of 0.70 V, which is approximately 250 mV less than the equilibrium overpotential of the Re(bpy-*t*Bu)$(CO)_3$Cl catalyst (0.95 V).[24]

CONCLUSIONS

We have described earth-abundant metal complexes, Mn(bpy-*t*Bu)$(CO)_3$Br (**1**) and [Mn(bpy-*t*Bu)$(CO)_3$(MeCN)](OTf) (**3**), that act as robust, selective, and efficient catalyst precursors for the reduction of CO_2 to CO. Complexes **1** and **3** resemble the Mn complexes studied by Deronzier and co-workers, and this work both confirms and extends their results. The addition of Brönsted acid is necessary for catalyst turnover in the Mn system, unlike in the analogous Re system. This difference may be due to the anodic shift of 300 mV for the second reduction of **1** compared to Re(bpy-*t*Bu)$(CO)_3$Cl. Three different weak acids were used (H_2O, MeOH, and TFE), and the catalytic current increases in cyclic voltammograms as the acid strength is increased. We were able to characterize both complex **1** and the active catalyst, $[Mn(bpy\text{-}tBu)(CO)_3]^-$ (**2**), by X-ray crystallography. The crystal structure of **2** is nearly identical to that of $[Re(bpy\text{-}tBu)(CO)_3]^-$ in geometry as well as in the DFT-calculated electronic structure. Infrared spectroelectrochemistry of complex **1** under nitrogen showed three distinct species. The first is the parent complex at rest, the second is Mn−Mn dimer formed by the first reduction and the immediate loss of bromide, and the third is the anionic species (**2**) that serves as the active catalyst for CO_2 reduction. A TOF of 340 s^{-1} was calculated for Mn catalyst **1** with 1.4 M TFE, corresponding to a Faradaic efficiency of 100 ± 15% for the formation of CO from CO_2, with no observable production of H_2. This activity is comparable to the corresponding Re catalysts at similar conditions. This class of carbon dioxide reduction electrocatalyst is exciting not only because of its ability to reduce CO_2 to CO at lower overpotentials than its Re counterpart, but also because of its earth-abundance, and significant potential for further improvement through synthetic modification.

EXPERIMENTAL SECTION

General Considerations. NMR spectra were recorded on a Jeol 500 MHz spectrometer at 298 K, and data were manipulated using Jeol Delta software. ^{1}H Chemical shifts are reported relative to TMS (δ = 0) and referenced against solvent residual peaks. Infrared spectra were collected on a Thermo Scientific Nicolet 6700 or a Bruker Equinox 55 spectrometer. Microanalyses were performed by Midwest Microlab, LLC (Indianapolis, IN) for C, H, and N.

Syntheses. Manipulations of Mn complexes were performed under an atmosphere of argon in the dark. Solvents were sparged with argon, dried on a custom dry solvent system over alumina columns, and stored over sieves before use. Potassium graphite (KC_8) was prepared by literature methods and stored at −30 °C in a drybox.[44] Tetrabutylammonium hexafluorophosphate (TBAH, Aldrich, 98%) was twice recrystallized from MeOH and dried under a vacuum at 90 °C overnight before use. 18-crown-6 was recrystallized from acetonitrile and dried under a vacuum at 90 °C overnight before use. Other reagents were used as received from the following: $Mn(CO)_5Br$ (Strem Chemical, 98%), 4,4′-di-*tert*-butyl-2,2′-bipyridine (Aldrich), and silver trifluoromethanesulfonate (AgOTf, Aldrich, 98%).

Synthesis of Mn(4,4′-di-*tert*-butyl-2,2′-bipyridine)$(CO)_3$Br (1). $Mn(CO)_5Br$ (500 mg, 1.82 mmol) was added to an argon-sparged Schlenk flask with 50 mL of Et_2O. 4,4′-Di-*tert*-butyl-2,2′-bipyridine (494 mg, 1.84 mmol) was added to the mixture, and the reaction was brought to reflux. The mixture quickly turned orange after reflux began and product began precipitating from the solution after 30 min. The reaction mixture was removed from heat after 1 h and submerged in a −80 °C acetone/dry ice bath. After 30 min in the cold bath, the reaction mixture was removed and the yellow solid was filtered and dried under a vacuum at 90 °C overnight. The yield of Mn(bpy-*t*Bu)$(CO)_3$Br was 601 mg (67%). ^{1}H NMR ($CDCl_3$): δ = 1.43 (br, 18 H, *t*Bu), 7.50 (br, 2 H, 5 and 5′ H's), 8.03 (br, 2 H, 6 and 6′ H's), 9.13 (br, 2 H, 3 and 3′ H's). IR (CH_3CN) ν(CO): 2028 cm^{-1}, 1933 cm^{-1}, 1923 cm^{-1}. Anal. Calcd for **1**, $C_{21}H_{24}BrMnN_2O_3$: C, 51.76; H, 4.96; N, 5.75. Found: C, 51.80; H, 4.95; N, 5.69.

Synthesis of [Mn(bpy-*t*Bu)$(CO)_3$][K(18-crown-6)] (2). One to ten millimolar solutions of Mn(4,4′-di-*tert*-butyl-2,2′-bipyridine)-$(CO)_3$Br were prepared in THF in an inert atmosphere and cooled to −35 °C. 18-crown-6 (2.5 equiv) and KC_8 (2.1 equiv) were added to the solution, and the solution was allowed to warm to room temperature over a period of 30 min. The solution was filtered, affording a deep purple solution of the anion. The solution was concentration from 20 mL to approximately 3 mL, and 17 mL of pentane was added. The solution was stored in the freezer overnight and was then decanted. The purple solid was dried under a vacuum (typical yield of 78%). X-ray quality crystals were grown from the vapor diffusion of pentane into a THF solution of the complex. ^{1}H NMR (THF-d_8): δ = 1.26 (s, 18 H, *t*Bu), 3.49 (br s, 24 H, K(18-crown-6)), 5.94 (d, 2 H, bpy, J_{H-H} = 6.9 Hz), 7.36 (s, 2 H, bpy), 9.27

dx.doi.org/10.1021/ic302391u | *Inorg. Chem.* 2013, 52, 2484−2491

(d, 2 H, bpy, J_{H-H} = 6.9 Hz). IR(THF) ν(CO): 1911 cm^{-1} and 1813 cm^{-1}.

Synthesis of [Mn(4,4′-di-*tert*-butyl-2,2′-bipyridine)-(CO)$_3$(MeCN)](OTf) (3). Complex **1** (500 mg, 1.02 mmol) was mixed with silver trifluoromethanesulfonate (AgOTf, 257 mg, 1.12 mmol) in a 200 mL Schlenk flask with 80 mL acetonitrile (MeCN) in the glovebox. The reaction flask was brought out of the box, covered with foil (to avoid exposure to light), and heated to reflux overnight. The reaction mixture was orange during reflux and had a black/brown solid at the bottom. After 18 h of reflux, the heat was removed. The solvent was removed by rotary evaporation, yielding an orange-brown mixture. The product was purified by flash chromatography with a Teledyne CombiFlash by passing the mixture through a basic alumina column with MeCN as the eluent. The fractions were combined, and the solvent was removed by rotary evaporation, yielding a bright orange solid. The final yield of pure product was 482 mg (79% yield). ^{1}H NMR ($CDCl_3$): δ = 1.45 (br, 18 H, *t*Bu), 2.36 (br, 3 H, bound MeCN), 7.58 (br, 2 H, bpy), 8.03 (br, 2 H, bpy), 9.13 (br, 2 H, bpy). IR (CH_3CN) ν(CO): 2047 cm^{-1}, 1955 cm^{-1} (br). Anal. Calcd for **1**, $C_{24}H_{27}F_3MnN_3O_6S$: C, 48.24; H, 4.55; N, 7.03. Found: C, 48.10; H, 4.47; N, 7.01.

Electrochemistry. Electrochemical experiments were performed using a BAS Epsilon potentiostat. A single-compartment cell was used for all cyclic voltammetry experiments with a glassy carbon electrode (1 mm in diameter from BASi), a Pt wire counter electrode, and a Ag/AgCl reference electrode separated from the solution by a Vycor tip. F_c/F_c^+ was added as an internal reference. All electrochemical experiments were performed with 0.1 M tetrabutylammonium hexafluorophosphate (TBAH) as the supporting electrolyte. Electrochemical cells were shielded from light during experiments. All solutions were purged with argon or CO_2 before CVs were taken. Mn complex concentrations ranged from 0.1−5.0 mM, and experiments with CO_2 were performed at gas saturation (~0.28 M) in acetonitrile. All potentials were converted from vs F_c^+/F_c to vs SCE by adding 380 mV to the potentials vs F_c^+/F_c.

Bulk Electrolysis. Bulk electrolysis experiments (at −2.2 V vs SCE) were carried out in a single-compartment cell designed in our laboratory. The setup included a 3 mm glassy carbon working electrode, a platinum wire counter electrode, and an Ag/AgCl reference electrode separated from the solution by a Vycor tip. A BAS Epsilon potentiostat was used to apply potential and record current. The bulk reductions were carried out in a CH_3CN with various amounts of added Brönsted acids and 0.1 M TBAH. Bulk electrolysis solutions were purged with CO_2 for 15 min prior to electrolysis. Solutions were constantly stirred and shielded from light throughout bulk electrolysis experiments. Gas analysis for bulk electrolysis experiments were performed using 1 mL sample injections on a Hewlett-Packard 7890A Series gas chromatograph with two molsieve columns (30 m × 0.53 mm ID × 25 μm film). The 1 mL injection was split between two columns, one with N_2 as the carrier gas and one with He carrier gas, in order to quantify both CO and H_2 simultaneously in each run. Gas chromatography calibration curves were made by sampling known volumes of CO and H_2 gas.

Infrared Spectroelectrochemistry (IR-SEC). The design of the IR spectroelectrochemical cell used for these studies has been reported previously by our group.[45] All spectroelectrochemical experiments were carried out in a 0.1 M TBAH solution using acetonitrile, and all solutions were prepared under an atmosphere of dry nitrogen in a glovebox. Blank acetonitrile solutions with 0.1 M TBAH were used for the FTIR solvent subtractions. A Pine Instrument Company model AFCBP1 bipotentiostat was used to affect and monitor thin layer bulk electrolysis.

X-ray Crystallographic Studies. The single crystal X-ray diffraction studies were carried out on a Bruker Kappa APEX-II CCD diffractometer equipped with Mo Kα radiation (λ = 0.71073 Å) or a Bruker Kappa APEX CCD diffractometer equipped with Cu Kα radiation (λ = 1.54184 Å). The crystals were mounted on a Cryoloop with Paratone oil and data were collected under a nitrogen gas stream at 100(2) K using ω and ϕ scans. Data were integrated using the Bruker SAINT software program and scaled using the SADABS software program. Solution by direct methods (SHELXS) produced a complete phasing model consistent with the proposed structure. All non-hydrogen atoms were refined anisotropically by full-matrix least-squares (SHELXL-97).[46] All hydrogen atoms were placed using a riding model. Their positions were constrained relative to their parent atom using the appropriate HFIX command in SHELXL-97. Crystallographic data and structure refinement parameters are summarized in Table 3 and S1.

Table 3. Crystallographic Data for Mn(bpy-*t*Bu)(CO)$_3$Br (1) and [Mn(bpy-*t*Bu)(CO)$_3$][K(18-crown-6)(THF)] (2)

	Mn(bpy-*t*Bu)(CO)$_3$Br (**1**)	[Mn(bpy-*t*Bu)(CO)$_3$][K(18-crown-6)(THF)] (**2**)
empirical formula	$C_{21}H_{24}BrMnN_2O_3$	$C_{74}H_{112}K_2Mn_2N_4O_{20}$
formula weight	487.27	1565.76
temperature (K)	100(2)	100(2)
wavelength (Å)	0.71073	1.54178
space group	$P2_1/n$ (No. 14)	$P2_1/n$ (No. 14)
a (Å)	13.5528(5)	18.2559(4)
b (Å)	17.1546(6)	18.4759(4)
c (Å)	19.1899(6)	24.2973(5)
α	90°	90°
β	96.8790(10)°	98.5560(10)°
γ	90°	90°
volume (Å^3)	4429.4(3)	8104.1(3)
Z	8	4
density$_{calcd}$ (Mg/m^3)	1.461	1.283
μ (mm^{-1})	2.423	4.023
R	0.0407	0.0733
R_w	0.1031	0.1941

DFT Calculations. Density functional theory calculations were performed with the Amsterdam Density Functional (ADF) program suite,[47,48] version 2007.01.[49] For all atoms, the triple-ζ Slater-type orbital TZ2P ADF basis set was utilized without frozen cores. Relativistic effects were included by use of the zeroth-order regular approximation (ZORA).[50,51] The functional used was BP86, and the local density approximation (LDA) of Vosko, Wilk and Nusair[52] (VWN) was coupled with the generalized gradient approximation (GGA) corrections described by Becke[53] and Perdew[54,55] for electron exchange and correlation, respectively. Single point frequency calculations were performed to verify that the geometries were at their minima. Molecular orbitals and final geometries were visualized with ADF-GUI.

■ ASSOCIATED CONTENT

Ⓢ Supporting Information

Additional details of the electrochemical studies of **1** and **3**, computational data for **2**, crystallographic data for **1** and **2**, and .cif files for **1** and **2**. This material is available free via the Internet at http://pubs.acs.org.

■ AUTHOR INFORMATION

Corresponding Author

*E-mail: ckubiak@ucsd.edu.

Notes

The authors declare no competing financial interest.

■ ACKNOWLEDGMENTS

The authors gratefully acknowledge the Defense Advanced Research Projects Agency (DARPA) through the Surface Catalysis (Surfcat) Program, and a grant from the Air Force

Office of Scientific Research through the MURI program (AFOSR Award No. FA9550-10-1-0572). We thank Prof. Arnie Rheingold and Dr. Curtis Moore for assistance with the X-ray crystallographic studies.

REFERENCES

(1) Ibrahim, H.; Ilinca, A.; Perron, J. *Renewable Sustainable Energy Rev.* **2008**, *12*, 1221.
(2) International Panel on Climate Change, Geneva, Switzerland, 2005.
(3) Zeman, F. *Environ. Sci. Technol.* **2007**, *41*, 7558.
(4) Stolaroff, J. K.; Keith, D. W.; Lowry, G. V. *Environ. Sci. Technol.* **2008**, *42*, 2728.
(5) Yu, K. M. K.; Curcic, I.; Gabriel, J.; Tsang, S. C. E. *ChemSusChem* **2008**, *1*, 893.
(6) Bhown, A. S.; Freeman, B. C. *Environ. Sci. Technol.* **2011**, *45*, 8624.
(7) Wang, T.; Lackner, K. S.; Wright, A. *Environ. Sci. Technol.* **2011**, *45*, 6670.
(8) Costentin, C.; Robert, M.; Savéant, J.-M. *Chem. Soc. Rev.* **2013**, DOI: 10.1039/C2CS35360A.
(9) Costentin, C.; Drouet, S.; Robert, M.; Savéant, J.-M. *Science* **2012**, *338*, 90.
(10) Inglis, J. L.; MacLean, B. J.; Pryce, M. T.; Vos, J. G. *Coord. Chem. Rev.* **2012**, *256*, 2571.
(11) Froehlich, J. D.; Kubiak, C. P. *Inorg. Chem.* **2012**, *51*, 3932.
(12) Benson, E. E.; Kubiak, C. P.; Sathrum, A. J.; Smieja, J. M. *Chem. Soc. Rev.* **2009**, *38*, 89.
(13) Schneider, J.; Jia, H.; Muckerman, J. T.; Fujita, E. *Chem. Soc. Rev.* **2012**, *41*, 2036.
(14) Kumar, B.; Llorente, M.; Froehlich, J.; Dang, T.; Sathrum, A.; Kubiak, C. P. *Annu. Rev. Phys. Chem.* **2012**, *63*, 541.
(15) Bernatis, P. R.; Miedaner, A.; Haltiwanger, R. C.; DuBois, D. L. *Organometallics* **1994**, *13*, 4835.
(16) DuBois, D. L.; Miedaner, A.; Haltiwanger, R. C. *J. Am. Chem. Soc.* **1991**, *113*, 8753.
(17) Raebiger, J. W.; Turner, J. W.; Noll, B. C.; Curtis, C. J.; Miedaner, A.; Cox, B.; DuBois, D. L. *Organometallics* **2006**, *25*, 3345.
(18) Steffey, B. D.; Curtis, C. J.; DuBois, D. L. *Organometallics* **1995**, *14*, 4937.
(19) Steffey, B. D.; Miedaner, A.; Maciejewski-Farmer, M. L.; Bernatis, P. R.; Herring, A. M.; Allured, V. S.; Carperos, V.; DuBois, D. L. *Organometallics* **1994**, *13*, 4844.
(20) Tanaka, K.; Ooyama, D. *Coord. Chem. Rev.* **2002**, *226*, 211.
(21) Slater, S.; Wagenknecht, J. H. *J. Am. Chem. Soc.* **1984**, *106*, 5367.
(22) Hawecker, J.; Lehn, J. M.; Ziessel, R. *J. Chem. Soc., Chem. Commun.* **1984**, 328.
(23) Kumar, B.; Smieja, J. M.; Kubiak, C. P. *J. Phys. Chem. C* **2010**, *114*, 14220.
(24) Smieja, J. M.; Kubiak, C. P. *Inorg. Chem.* **2010**, *49*, 9283.
(25) Sullivan, B. P.; Bolinger, C. M.; Conrad, D.; Vining, W. J.; Meyer, T. J. *J. Chem. Soc., Chem. Commun.* **1985**, 1414.
(26) Kumar, B.; Smieja, J. M.; Sasayama, A. F.; Kubiak, C. P. *Chem. Commun.* **2012**, *48*, 272.
(27) Smieja, J. M.; Benson, E. E.; Kumar, B.; Grice, K. A.; Seu, C. S.; Miller, A. J. M.; Mayer, J. M.; Kubiak, C. P. *Proc. Natl. Acad. Sci. U.S.A.* **2012**, *109*, 15646.
(28) *CRC Handbook of Chemistry and Physics*; 92nd ed.; Haynes, W. M., Ed.; CRC Press: Boca Raton, FL, 2011−2012.
(29) Bourrez, M.; Molton, F.; Chardon-Noblat, S.; Deronzier, A. *Angew. Chem., Int. Ed.* **2011**, *50*, 9903.
(30) Staal, L. H.; Oskam, A.; Vrieze, K. *J. Organomet. Chem.* **1979**, *170*, 235.
(31) Benson, E. E.; Kubiak, C. P. *Chem. Commun.* **2012**, *48*, 7374.
(32) Addison, A. W.; Rao, T. N.; Reedijk, J.; van Rijn, J.; Verschoor, G. C. *J. Chem. Soc., Dalton Trans.* **1984**, 1349.
(33) Hartl, F.; Rosa, P.; Ricard, L.; Le Floch, P.; Záliš, S. *Coord. Chem. Rev.* **2007**, *251*, 557.
(34) Gore-Randall, E.; Irwin, M.; Denning, M. S.; Goicoechea, J. M. *Inorg. Chem.* **2009**, *48*, 8304.
(35) Wang, J. *Analytical Electrochemistry*, 3rd ed.; John Wiley & Sons, Inc.: Hoboken, NJ, 2006.
(36) Johnson, F. P. A.; George, M. W.; Hartl, F.; Turner, J. J. *Organometallics* **1996**, *15*, 3374.
(37) Hartl, F.; Mahabiersing, T.; Le Floch, P.; Mathey, F.; Ricard, L.; Rosa, P.; Záliš, S. *Inorg. Chem.* **2003**, *42*, 4442.
(38) Bard, A. J.; Faulkner, L. R. *Electrochemical Methods: Fundamentals and Applications*, 2nd ed.; Wiley: New York, 2001.
(39) Haines, R. J.; Wittrig, R. E.; Kubiak, C. P. *Inorg. Chem.* **1994**, *33*, 4723.
(40) Hartl, F.; Rossenaar, B. D.; Stor, G. J.; Stufkens, D. J. *Recl. Trav. Chim. Pays-Bas* **1995**, *114*, 565.
(41) Gennaro, A.; Isse, A. A.; Vianello, E. *J. Electroanal. Chem.* **1990**, *289*, 203.
(42) Wong, K.-Y.; Chung, W.-H.; Lau, C.-P. *J. Electroanal. Chem.* **1998**, *453*, 161.
(43) Costentin, C.; Drouet, S.; Robert, M.; Savéant, J.-M. *J. Am. Chem. Soc.* **2012**, *134*, 11235.
(44) Schwindt, M. A.; Lejon, T.; Hegedus, L. S. *Organometallics* **1990**, *9*, 2814.
(45) Zavarine, I. S.; Kubiak, C. P. *J. Electroanal. Chem.* **2001**, *495*, 106.
(46) Sheldrick, G. *Acta Crystallogr., Sect. A* **2008**, *64*, 112.
(47) te Velde, G.; Bickelhaupt, F. M.; Baerends, E. J.; Fonseca Guerra, C.; van Gisbergen, S. J. A.; Snijders, J. G.; Ziegler, T. *J. Comput. Chem.* **2001**, *22*, 931.
(48) Fonseca Guerra, C.; Snijders, J. G.; te Velde, G.; Baerends, E. *J. Theor. Chem. Acc.* **1998**, *99*, 391.
(49) ADF2007.01; SCM, *Theoretical Chemistry*: Vrije Universiteit, Amsterdam, The Netherlands, http://www.scm.com.
(50) van Lenthe, E.; Baerends, E. J.; Snijders, J. G. *J. Chem. Phys.* **1993**, *99*, 4597.
(51) van Lenthe, E.; Snijders, J. G.; Baerends, E. J. *J. Chem. Phys.* **1996**, *105*, 1200.
(52) Vosko, S. H.; Wilk, L.; Nusair, M. *Can. J. Phys.* **1980**, *58*, 1200.
(53) Becke, A. D. *Phys. Rev. A* **1988**, *38*, 3098.
(54) Perdew, J. P. *Phys. Rev. B* **1986**, *33*, 8822.
(55) Perdew, J. P. *Phys. Rev. B* **1986**, *34*, 7406.